Korea-Australia Rheology Journal
Vol. 17, No. 2, June 2005 pp. 47-62

Dynamic response of heat and mass transfer in blood flow through stenosed bifurcated arteries

S. Chakravarty* and S. Sen
Department of Mathematics, Visva-Bharati University, Santiniketan 731 235, India
(Received December 18, 2004; final revision received April 28, 2005)

Abstract

The present study deals with a mathematical model describing the dynamic response of heat and mass transfer in blood flow through bifurcated arteries under stenotic condition. The geometry of the bifurcated arterial segment possessing constrictions in both the parent and the daughter arterial lumen frequently appearing in the diseased arteries causing malfunction of the cardiovascular system, is formulated mathematically with the introduction of the suitable curvatures at the lateral junction and the flow divider. The blood flowing through the artery is treated to be Newtonian. The nonlinear unsteady flow phenomena is governed by the Navier-Stokes equations while those of heat and mass transfer are controlled by the heat conduction and the convection-diffusion equations respectively. All these equations together with the appropriate boundary conditions describing the present biomechanical problem following the radial coordinate transformation are solved numerically by adopting finite difference technique. The respective profiles of the flow field, the temperature and the concentration and their distributions as well are obtained. The influences of the stenosis, the arterial wall motion and the unsteady behaviour of the system in terms of the heat and mass transfer on the blood stream in the entire arterial segment are highlighted through several plots presented at the end of the paper in order to illustrate the applicability of the present model under study.

1. Introduction

In the recent past, the study of the influence of heat and mass transfer on biofluids has become quite interesting to many researchers both from the theoretical and experimental or clinical point of view. Hemodynamics has long been suspected of being involved in arterial lesions leading to the malfunction of the cardiovascular system resulting from the normal flow disturbances around bends and curvatures in larger arteries where plaques are frequently formed. The heat and mass transport phenomena of blood always play a key role to the understanding and development of arterial diseases in general and the heat flow together with the transport of macromolecules with dissolved gases to and through the arterial wall influence more on the growth and development of atherogenetic processes, in particular. It is well established that large blood vessels perturb the induced temperature distributions in physiological situations. The understandings of the magnitude of the perturbation of the temperature distribution as a function of the vessel diameter and temperature gradient are critical to the development of appropriate models of bioheat transport.

In the past, there has been a number of studies to examine heat transfer in blood vessels. Charm *et al.* (1968) experimentally investigated heat transfer in small tubes of diameter 0.6 mm in a water bath, while Victor and Shah (1975; 1976) computed heat transfer for uniform heat flux and uniform wall temperature cases for fully developed flow and in the entrance region. The correlation equations for estimating the heat transfer under different configurations and diameters of blood vessels were developed by Chato (1980). Based upon the considerations of laminar and fully thermally developed flow in large blood vessels, Lagendijk (1982) analysed temperature distributions in the entrance region around the vessels during hyperthemia. Barozzi and Dumas (1991) calculated heat transfer in the entrance region considering the rheological properties of the blood stream and a cell free peripheral plasma layer at the vessel wall. All these studies concentrated only on the heat transfer to blood flowing through the arteries but disregarded mass transport processes. There could have been many reasons behind not carrying out such investigations. One possible reason could be that of the problems of mass transport phenomena are highly convection dominated

*Corresponding author: santabrata2004@yahoo.co.in

because of the low diffusion coefficients of the principal constituents governing transportation of blood.

An introductory attempt to investigate the convective effect of steady blood flow on diffusion processes in an arterial system has been made by Friedman and Ehrlich (1975). They studied the flow in a simplified two dimensional arterial bifurcation and obtained an analytical boundary layer solution for the concentration of the solute at the vessel wall. Back *et al.* (1997) investigated pulsatile oxygen transport to multiple non-constricted plaque regions quantitatively by employing finite difference technique and indicated a strong reduction in oxygen transport on the rear end of plaques at incipient flow separation zones. Another numerical simulation of mass transfer in a sudden expansion tube model under pulsatile conditions was performed by Ma *et al.* (1994) where the influence of separated flow on luminal mass transport and the vessel wall mass transfer coefficient was recorded. It has been known that in the arterial system, the hemodynamic factors affect significantly blood phase transport and the vessel wall characteristics. Hence the simultaneous treatment of the luminal transport in blood phase and shear dependent variations in initimal permeability becomes important for an understanding of the mass transport phenomena. In this context, Rappitsch and Perktold (1996) studied numerically the steady convective diffusion processes in an axisymmetric tube having a local constriction by applying a passive transport law for the flux at the wall and physiologically realistic values for the flow and mass transfer parameters.

To the authors' knowledge, there has been quite a good number of studies (Mathur and Bhatnagar, 1967; Kawase and Ulbrecht, 1983; Parikh and Mahalingam, 1988; Pereira *et al.*, 1989; Hung and Perng, 1991; Ahmed and Attia, 1998) concerning heat and mass transfer in non-Newtonian fluids where the governing flow is mostly considered to be steady and the influence of the non-Newtonian parameters on the flow field and the temperature field were mostly recorded. It is commonly believed that the effect of non-Newtonian property of blood is small in the larger arteries where the shear rate is high. The studies mentioned above were not performed in bifurcated arteries under stenotic conditions although the flow phenomena in the aortic bifurcation is of great clinical interest both with respect to genesis and the diagnostics of atherosclerosis. The arterial constrictions usually appear around curvatures, junctions and bifurcations of large and medium arteries, where the flow patterns are essentially complicated. The complex flow disorder poses great concern to distinguish these disturbances from normal flow behaviour in these regions.

Keeping in view of the motivation as stated above, a sincere attempt is made to formulate an unsteady two dimensional constricted bifurcated artery theoretically in the present investigation in order to estimate some of the important characteristics of heat and mass transfer phenomena governing pulsatile blood flow in aortic bifurcation. The time-variant geometry of the bifurcated artery developed by Chakravarty and Mandal (1997) has been updated further for the present requirement. The symmetrical aorta is assumed to have a couple of constrictions -- - one in the parent arterial lumen and the other in the daughter one. The flowing blood contained in the bifurcated artery is considered to be Newtonian. The cylindrical coordinate system has been taken for analytical formulation. Due attention has also been paid to the effect of arterial wall motion on local fluid mechanics but not on the stresses and the strains in the vascular wall. The unsteady nonlinear Navier - Stokes equations of motion governing blood flow, the heat flow and the mass transport equations coupled to the velocity field are taken up along with the appropriate initial and boundary conditions in order to define the present biomechanical problem. Following the radial coordinate transformation, these equations are reduced to a tractable form initially and then they are solved numerically by employing a suitable finite difference technique with the use of boundary and matching conditions in concert with the physical representation of the problem. A thorough quantitative analysis has finally been performed at the end of the paper through graphical representations of the results together with their discussion at length in order to validate the applicability of the present mathematical model.

2. Formulation of the problem

The formulation of the mathematical model under consideration is based on the following realistic assumptions in order to update the present model one step closer to the real situation:

- The arteries forming bifurcations are symmetrical about the axis of the trunk and cylinders of finite length having 90° bifurcation
- Both the parent aorta and its daughter arteries possess a mild stenosis each in their lumen
- The flow is treated to be unsteady and two dimensional so that both the radial and the axial velocity components come into play
- The heat and mass transport equations are individually coupled to the velocity field of the blood stream
- The streaming blood is treated to be a homogenous Newtonian fluid of constant density
- The arterial wall distensibility is introduced into the local fluid mechanics but not on the stresses and the strains on the vessel wall
- The suitable curvatures are introduced at the lateral junctions and the flow divider of the arterial bifurcation in order to get away from any discontinuity causing large flow separation zones or non-existent flow separation zones.

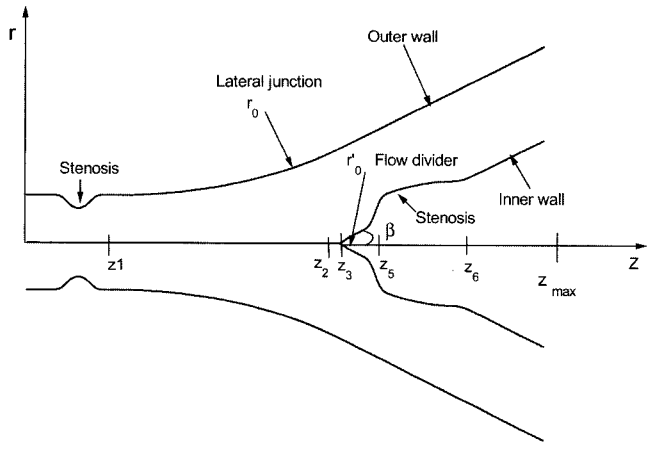

Fig. 1. Schematic diagram of the constricted bifurcated arterial segment.

Let (r, θ, z) be the coordinates of the representative material point in the cylindrical polar coordinate system where the z-axis is taken along the axis of the trunk while (r, θ) are taken along the radial and the circumferential directions respectively. The geometry of the bifurcated artery (cf. Fig. 1) having two symmetrical mild stenoses ---- one in the parent arterial lumen and the other in its branch is constructed mathematically of which the outer wall geometry is described by

$$R_1(z,t)=\begin{cases} a.a_1(t), & 0\le z\le d',\ d'+l_0\le z\le z_1,\\ \left[a-\dfrac{4\tau_m}{l_0^2}\{l_0(z-d')-(z-d')^2\}\right]a_1(t), & d'\le z\le d'+l_0,\\ [a+r_0-\sqrt{r_0^2-(z-z_1)^2}]a_1(t), & z_1\le z\le z_2,\\ [2r_1\sec\beta+(z-z_2)\tan\beta]a_1(t), & z_2\le z\le z_{max}, \end{cases} \tag{1}$$

while that for the inner wall is given by

$$R_2(z,t)=\begin{cases} 0, & 0\le z\le z_3,\\ \sqrt{r_0'^2-(z-z_3-r_0')^2}\,b_1(t), & z_3\le z\le z_3+r_0'\,(1-\sin\beta),\\ (z-z_2)\tan\beta b_1(t), & z_3+r_0'\,(1-\sin\beta)\le z\le z_5, z_6\le z\le z_{max},\\ \sqrt{r_2'^2-(z_6-z)^2}\,b_1(t), & z_5\le z\le z_6, \end{cases} \tag{2}$$

where $R_1(z, t)$ and $R_2(z, t)$ are the respective radii of the outer and the inner wall, a the unconstricted radius of the parent aorta, r_1 the radius of the daughter artery, (r_0, r_0') the respective radii of curvatures for the lateral junction and the flow divider, l_0 the length of the stenosis at a distance d' from the origin, (z_1, z_2) the locations of the onset and the offset of the lateral junction, z_3 the apex, (z_5, z_6) the respective sites corresponding to the onset and offset of the stenosis in the daughter artery, β be the semi-bifurcation angle and τ_m designates the height of the stenosis. Here z_{max} is chosen to be the finite length of the bifurcated artery.

The various parameters involved in the above expressions (1) and (2) may be defined as

$$a_1(t)=1-(\cos\omega t-1)k_1\exp(-k_1\omega t),$$

$$b_1(t)=\frac{1}{a_1(t)},$$

$$z_2=z_1+(a-2r_1\sec\beta)\frac{\sin\beta}{\cos\beta-1},$$

$$r_0=\frac{a-2r_1\sec\beta}{\cos\beta-1},\qquad r_0'=\frac{(z_3-z_2)\sin\beta}{1-\sin\beta},$$

$$r_2'=(z_6-z_2)\tan\beta \tag{3}$$

and $z_3=z_2+q$, where q is chosen to be a small number lying in the range $0.1\le q\le 0.5$ for the geometrical compatibility and k_1 is a constant. The choice of the time-variant function $a_1(t)$ reflects closely the pulsatile nature of the blood flow which is oscillatory and such oscillation damps out with large time advancement resulting in the artery with unconstrained radius only.

The Navier-Stokes' equations and the equation of continuity that govern the unsteady nonlinear fully developed swirl free flow of an incompressible Newtonian fluid representing blood may be written as

$$\rho\left(\frac{\partial u}{\partial t}+u\frac{\partial u}{\partial r}+w\frac{\partial u}{\partial z}\right)=-\frac{\partial p}{\partial r}+\mu\left(\frac{\partial^2 u}{\partial r^2}+\frac{1}{r}\frac{\partial u}{\partial r}-\frac{u}{r^2}+\frac{\partial^2 u}{\partial z^2}\right), \tag{4}$$

$$\rho\left(\frac{\partial w}{\partial t}+u\frac{\partial w}{\partial r}+w\frac{\partial w}{\partial z}\right)=-\frac{\partial p}{\partial z}+\mu\left(\frac{\partial^2 w}{\partial r^2}+\frac{1}{r}\frac{\partial w}{\partial r}+\frac{\partial^2 w}{\partial z^2}\right) \tag{5}$$

and $$\frac{\partial u}{\partial r}+\frac{u}{r}+\frac{\partial w}{\partial z}=0, \tag{6}$$

where $u=u(r, z, t)$ and $w=w(r, z, t)$ are the radial and the axial velocity components of the streaming blood respectively, p the pressure, ρ the density and μ represents the viscosity of blood.

The heat conduction and the convection-diffusion equations governing the flow of heat and mass transport in the blood stream each coupled to the fluid velocity field are given by

$$\rho\, c_p\frac{\partial T}{\partial t}=k\nabla^2 T+2\mu\left(\frac{\partial^2 w}{\partial z^2}+\frac{\partial^2 u}{\partial r^2}+\frac{\partial w}{\partial r}+\frac{\partial u}{\partial z}\right) \tag{7}$$

and

$$\frac{\partial c}{\partial t}+u\frac{\partial c}{\partial r}+w\frac{\partial c}{\partial z}=D\left(\frac{\partial^2 c}{\partial z^2}+\frac{1}{r}\frac{\partial c}{\partial r}+\frac{\partial^2 c}{\partial r^2}\right)+\frac{Dk_T}{T_m}\left(\frac{\partial^2 T}{\partial z^2}+\frac{1}{r}\frac{\partial T}{\partial r}+\frac{\partial^2 T}{\partial r^2}\right), \tag{8}$$

in which T is the temperature, c_p the specific heat of the streaming blood at constant pressure, k the thermal conductivity, c the solute or gas-concentration, D the constant coefficient of diffusion, k_T the thermal diffusion ratio and T_m represents the mean blood temperature. The second term on the right hand side of (8) indicates the influences

of non isothermal character of the blood stream on the mass transportation of oxygen.

Moreover, the pumping action of the heart is represented by the input pressure gradient appearing in (5) produced by it, the form of which has been taken from Burton (1966) as

$$-\frac{\partial p}{\partial z} = A_0 + A_1 \cos \omega t, \tag{9}$$

where A_0 is the constant amplitude of the pressure gradient, A_1 is the amplitude of the pulsatile component giving rise to systolic and diastolic pressure. Here $\omega = 2\pi f_p$, f_p being the pulse frequency.

3. Initial and boundary conditions

It is assumed that there is a non-null velocity field of the streaming blood having a constant temperature when the entire system is at rest, that means initially

$$u(r, z, 0) = u_0,\ w(r, z, 0) = w_0 \text{ and } T(r, z, 0) = T_0. \tag{10}$$

As no radial flow of blood takes place along the axis of the parent aorta and there is no shear rate of the fluid along the axis of the trunk, one may write as

$$u(r,z,t) = 0,\ \frac{\partial w(r,z,t)}{\partial r} = 0 \text{ on } r = 0 \text{ for } 0 \le z \le z_3. \tag{11}$$

The velocity boundary conditions of the blood stream on the outer arterial wall surface are taken as

$$u(r,z,t) = \alpha \frac{\partial R_1}{\partial t},\ w(r,z,t) = 0 \text{ on } r = R_1(z, t) \text{ for all } z, \tag{12}$$

while those of the inner half (daughter) are assumed to be

$$u(r,z,t) = \alpha \frac{\partial R_2}{\partial t},\ w(r,z,t) = 0 \text{ on } r = R_2(z, t) \text{ for } z \ge z_3 \tag{13}$$

in which $\alpha = 1$ for $z < z_3$ and $\alpha = \sec\beta$ for $z \ge z_3$.

The axial symmetry conditions for the temperature and mass concentration are introduced as

$$\frac{\partial T(r,z,t)}{\partial r} = 0,\ \frac{\partial c(r,z,t)}{\partial r} = 0 \text{ on } r = 0 \text{ for } 0 \le z \le z_3. \tag{14}$$

At the inlet, the concentration of the solute is assumed to be constant while the concentration gradient at the outlet may be assumed to be equal to zero, that is

$$c(r, z, t) = c_0 \text{ at } z = 0 \text{ and } \frac{\partial c(r,z,t)}{\partial z} = 0 \text{ at } z = z_3. \tag{15}$$

Moreover, it is assumed that there is an uniform temperature at the outer arterial wall surface, that is

$$T(r, z, t) = T_1 \text{ on } r = R_1(z, t) \text{ for all } z. \tag{16}$$

4. Method of solution

Let us introduce a radial coordinate transformation, given by

$$\xi = \frac{r - R_2}{R_1 - R_2} = \frac{r - R_2}{R}, \tag{17}$$

which possesses the effect of immobilizing the bifurcated arterial wall in the transformed coordinate ξ. Here $R = R(z, t) = R_1(z, t) - R_2(z, t)$.

Using this transformation, the equations (5)-(8) take the following form

$$\begin{aligned}\frac{\partial w}{\partial t} = &-\frac{1}{\rho}\frac{\partial p}{\partial z} + \frac{1}{R}\frac{\partial w}{\partial \xi}\left[\left(\xi\frac{\partial R}{\partial t} + \frac{\partial R_2}{\partial t}\right) + \frac{\mu}{\rho(\xi R + R_2)}\right.\\ &\left.-\frac{\mu}{\rho}\left\{\frac{\partial^2 R_2}{\partial z^2} + \xi\frac{\partial^2 R}{\partial z^2} - \frac{2}{R}\frac{\partial R}{\partial z}\left(\xi\frac{\partial R}{\partial z} + \frac{\partial R_2}{\partial z}\right)\right\}\right]\\ &+\frac{\mu}{\rho R^2}\left[1 + \left(\xi\frac{\partial R}{\partial z} + \frac{\partial R_2}{\partial z}\right)^2\right]\frac{\partial^2 w}{\partial \xi^2} - \frac{1}{R}u\frac{\partial w}{\partial \xi}\\ &-w\left[\frac{\partial w}{\partial z} - \frac{1}{R}\left(\xi\frac{\partial R}{\partial z} + \frac{\partial R_2}{\partial z}\right)\frac{\partial w}{\partial \xi}\right] + \frac{\mu}{\rho}\frac{\partial^2 w}{\partial z^2},\end{aligned} \tag{18}$$

$$\frac{1}{R}\frac{\partial u}{\partial \xi} + \frac{u}{(\xi R + R_2)} + \frac{\partial w}{\partial z} - \frac{1}{R}\frac{\partial w}{\partial \xi}\left(\xi\frac{\partial R}{\partial z} + \frac{\partial R_2}{\partial z}\right) = 0, \tag{19}$$

$$\begin{aligned}\frac{\partial T}{\partial t} = &\left[\frac{1}{R}\left(\xi\frac{\partial R}{\partial t} + \frac{\partial R_2}{\partial t}\right) + \frac{w}{R}\left(\xi\frac{\partial R}{\partial z} + \frac{\partial R_2}{\partial z}\right) - \frac{u}{R}\right.\\ &\left.+\frac{k}{\rho c_p R}\left\{\frac{1}{\xi R + R_2} + \frac{2}{R}\left(\xi\frac{\partial R}{\partial z} + \frac{\partial R_2}{\partial z}\right)\frac{\partial R}{\partial z} - \left(\xi\frac{\partial^2 R}{\partial z^2} + \frac{\partial^2 R_2}{\partial z^2}\right)\right\}\right]\frac{\partial T}{\partial \xi}\\ &-w\frac{\partial T}{\partial z} + \frac{k}{\rho c_p R^2}\left\{1 + \left(\xi\frac{\partial R}{\partial z} + \frac{\partial R_2}{\partial z}\right)^2\right\}\frac{\partial^2 T}{\partial \xi^2} + \frac{k}{\rho c_p}\frac{\partial^2 T}{\partial z^2}\\ &+\frac{2\mu}{\rho c_p}\left[\left\{\frac{2}{R^2}\left(\xi\frac{\partial R}{\partial z} + \frac{\partial R_2}{\partial z}\right)\frac{\partial R}{\partial z} - \frac{1}{R}\left(\xi\frac{\partial^2 R}{\partial z^2} + \frac{\partial^2 R_2}{\partial z^2}\right) + \frac{1}{R}\right\}\frac{\partial w}{\partial \xi}\right.\\ &+\frac{1}{R^2}\left(\xi\frac{\partial R}{\partial z} + \frac{\partial R_2}{\partial z}\right)^2\frac{\partial^2 w}{\partial \xi^2} + \frac{\partial^2 w}{\partial z^2}\\ &\left.-\frac{1}{R}\left(\xi\frac{\partial R}{\partial z} + \frac{\partial R_2}{\partial z}\right)\frac{\partial u}{\partial \xi} + \frac{1}{R^2}\frac{\partial^2 u}{\partial \xi^2} + \frac{\partial u}{\partial z}\right]\end{aligned} \tag{20}$$

and

$$\begin{aligned}\frac{\partial c}{\partial t} = &\left[\frac{1}{R}\left(\xi\frac{\partial R}{\partial t} + \frac{\partial R_2}{\partial t}\right) + \frac{w}{R}\left(\xi\frac{\partial R}{\partial z} + \frac{\partial R_2}{\partial z}\right) - \frac{u}{R} + \frac{2D}{R^2}\left(\xi\frac{\partial R}{\partial z} + \frac{\partial R_2}{\partial z}\right)\frac{\partial R}{\partial z}\right.\\ &\left.-\frac{D}{R}\left(\xi\frac{\partial^2 R}{\partial z^2} + \frac{\partial^2 R_2}{\partial z^2}\right) + \frac{D}{R(\xi R + R_2)}\right]\frac{\partial c}{\partial \xi} + \frac{D}{R^2}\left[1 + \left(\xi\frac{\partial R}{\partial z} + \frac{\partial R_2}{\partial z}\right)^2\right]\frac{\partial^2 c}{\partial \xi^2}\\ &-w\frac{\partial c}{\partial z} + D\frac{\partial^2 c}{\partial z^2} + \frac{Dk_t}{T_m}\left[\left\{\frac{2}{R^2}\left(\xi\frac{\partial R}{\partial z} + \frac{\partial R_2}{\partial z}\right)\frac{\partial R}{\partial z} - \frac{1}{R}\left(\xi\frac{\partial^2 R}{\partial z^2} + \frac{\partial^2 R_2}{\partial z^2}\right)\right.\right.\\ &\left.\left.+\frac{1}{R(\xi R + R_2)}\right\}\frac{\partial T}{\partial \xi} + \frac{1}{R^2}\left\{1 + \left(\xi\frac{\partial R}{\partial z} + \frac{\partial R_2}{\partial z}\right)^2\right\}\frac{\partial^2 T}{\partial \xi^2} + \frac{\partial^2 T}{\partial z^2}\right]\end{aligned} \tag{21}$$

Since the radius of the artery is considered to be much smaller than its length and the variation of radius is small for mild stenosis, the pressure variation within the arterial cross section is negligible and hence the radial Navier-Stokes equation (4) may be disregarded. Although the effect of arterial stenosis and branching on the motion of blood is important because of convective acceleration, its effect on the radial motion of the artery is negligible. Because of the small radial velocity and acceleration, the radial variation of pressure within the artery can also be neglected. Such an assumption is well established and authenticated by many investigators (cf. Womersley, 1957; Ling and Atabek, 1972; Imaeda and Goodman, 1980; Deshpande *et al.*, 1976; Pedley, 1980).

The transformed initial and boundary conditions corresponding to (10)-(16) with the introduction of (17) should have following form

$$u(\xi, z, 0) = u_0,\ w(\xi, z, 0) = w_0,\ T(\xi, z, 0) = T_0 \tag{22}$$

$$u(\xi,z,t)=0,\ \frac{\partial w(\xi,z,t)}{\partial \xi}=0 \ \text{ on } \xi=0 \text{ for } 0\le z\le z_3 \tag{23}$$

$$u(\xi,z,t)=\alpha\frac{\partial R_1}{\partial t},\ w(\xi,z,t)=0 \ \text{ on } \xi=1 \text{ for all } z \tag{24}$$

$$u(\xi,z,t)=\alpha\frac{\partial R_2}{\partial t},\ w(\xi,z,t)=0 \ \text{ on } \xi=0 \text{ for } z\ge z_3 \tag{25}$$

$$\frac{\partial T(\xi,z,t)}{\partial \xi}=0,\ \frac{\partial c(\xi,z,t)}{\partial \xi}=0 \ \text{ on } \xi=0 \text{ for } 0\le z\le z_3 \tag{26}$$

$$c(\xi, z, t) = c_0 \text{ at } z=0, \text{ and } \frac{\partial c(\xi,z,t)}{\partial z}=0 \text{ at } z=z_3 \tag{27}$$

$$\text{and } T(\xi, z, t) = T_1 \text{ on } \xi=1 \text{ for all } z. \tag{28}$$

First the equations governing blood flow are solved which are subsequently used to solve the heat conduction equation and finally the convection diffusion equation by exploiting the respective boundary and the initial conditions. In order to make the equations (18) and (19) tractable, we multiply both sides of (19) by $\xi R + R_2$ and integrate with respect to ξ so that we have

$$\begin{aligned} u(\xi,z,t) &= \left(\xi\frac{\partial R}{\partial z}+\frac{\partial R_2}{\partial z}\right)w(\xi,z,t)+\frac{R_2}{\xi R+R_2}u(0,z,t) \\ &\quad -\frac{R_2}{\xi R+R_2}\int_0^{\xi}(\xi R+R_2)\frac{\partial w}{\partial z}d\xi \\ &\quad -\frac{1}{\xi R+R_2}\int_0^{\xi}\left(2\xi R\frac{\partial R}{\partial z}+R_2\frac{\partial R}{\partial z}+R\frac{\partial R_2}{\partial z}\right)w d\xi \end{aligned} \tag{29}$$

Using the boundary condition (24), the equation (29) may take the following form

$$\begin{aligned} -\int_0^1(\xi R+R_2)\frac{\partial w}{\partial z}d\xi &= \int_0^1\left[\left(2\xi\frac{\partial R}{\partial z}+\frac{R_2}{R}\frac{\partial R}{\partial z}+\frac{\partial R_2}{\partial z}\right)w \right. \\ &\quad \left. +\frac{R_1}{R}\left\{\alpha\frac{\partial R_1}{\partial t}-\frac{R_2}{R_1}u(0,z,t)\right\}f(\xi)\right]d\xi \end{aligned}$$

where $f(\xi)$ is an arbitrary function satisfying $\int_0^1 f(\xi)d\xi = 1$.

The approximation has been used consisting of the equality between the integrals to integrands. In other words, we suppose that the arbitrary function $f(\xi)$ exists so that

$$\begin{aligned} &(\xi R+R_2)\frac{\partial w}{\partial z}+\left(2\xi\frac{\partial R}{\partial z}+\frac{R_2}{R}\frac{\partial R}{\partial z}+\frac{\partial R_2}{\partial z}\right)w \\ &\quad +\frac{R_1}{R}\left\{\alpha\frac{\partial R_1}{\partial t}-\frac{R_2}{R_1}u(0,z,t)\right\}f(\xi)=0 \end{aligned}$$

The function $f(\xi)$ must also satisfy the condition $f(1) = 0$ because it has to be $\left.\frac{\partial w}{\partial z}\right|_{\xi=1} = 0$. Without any loss of generality one can assume $f(\xi) = -4\xi(\xi^2 - 1)$ which satisfies all the necessary conditions mentioned above.

Thus the above relation becomes

$$\begin{aligned} u(\xi,z,t) &= \left(\xi\frac{\partial R}{\partial z}+\frac{\partial R_2}{\partial z}\right)w(\xi,z,t)+\frac{R_2}{\xi R+R_2}u(0,z,t) \\ &\quad +\frac{\xi^2 R_1}{\xi R+R_2}\left\{\alpha\frac{\partial R_1}{\partial t}-\frac{R_2}{R_1}u(0,z,t)\right\}(2-\xi^2) \end{aligned} \tag{30}$$

Introducing (30) into (18) one obtains

$$\begin{aligned} \frac{\partial w}{\partial t} &= -\frac{1}{\rho}\frac{\partial p}{\partial z}+\frac{1}{R}\frac{\partial w}{\partial \xi}\left[\left(\xi\frac{\partial R}{\partial t}+\frac{\partial R_2}{\partial t}\right)+\frac{\mu}{\rho(\xi R+R_2)}-\frac{\mu}{\rho}\left\{\frac{\partial^2 R_2}{\partial z^2}+\xi\frac{\partial^2 R}{\partial z^2}\right.\right. \\ &\quad \left.-\frac{2}{R}\frac{\partial R}{\partial z}\left(\xi\frac{\partial R}{\partial z}+\frac{\partial R_2}{\partial z}\right)\right\}-\frac{R_2}{\xi R+R_2}u(0,z,t)-\frac{\xi^2 R_1}{\xi R+R_2}\left\{\alpha\frac{\partial R_1}{\partial t}\right. \\ &\quad \left.\left.-\frac{R_2}{R_1}u(0,z,t)\right\}(2-\xi^2)\right]+\frac{\mu}{\rho R^2}\left[1+\left(\xi\frac{\partial R}{\partial z}+\frac{\partial R_2}{\partial z}\right)^2\right]\frac{\partial^2 w}{\partial \xi^2} \\ &\quad +\frac{\mu}{\rho}\frac{\partial^2 w}{\partial z^2}-w\frac{\partial w}{\partial z} \end{aligned} \tag{31}$$

The present tractable form of (30) and (31) are now solved numerically by using finite difference technique following the stated boundary conditions. Subsequently, the coupled heat conduction equation (20) is solved numerically by making use of the numerical flow velocity field thus obtained. Finally the coupled mass transport equation (21) can be solved numerically with the knowledge of the quantitative estimates of the flow field and the temperature distribution just obtained.

5. Finite difference approximation

The finite difference scheme used to solve the equations (30), (31), (20) and (21) subject to the initial and the boundary conditions (22)-(28) is based on the forward difference representations for the time derivatives and the central difference formulation for the spatial derivatives in

the following manner :

$$\frac{\partial w}{\partial t}=\frac{w_{i,j}^{k+1}-w_{i,j}^{k}}{\Delta t},\ \frac{\partial w}{\partial \xi}=\frac{w_{i,j+1}^{k}-w_{i,j-1}^{k}}{2\Delta\xi},$$
$$\frac{\partial w}{\partial z}=\frac{w_{i+1,j}^{k}-w_{i-1,j}^{k}}{2\Delta z},\ \frac{\partial^2 w}{\partial z^2}=\frac{w_{i+1,j}^{k}-2w_{i,j}^{k}+w_{i-1,j}^{k}}{(\Delta z)^2},$$
$$\frac{\partial T}{\partial t}=\frac{T_{i,j}^{k+1}-T_{i,j}^{k}}{\Delta t},\ \frac{\partial T}{\partial \xi}=\frac{T_{i,j+1}^{k}-T_{i,j-1}^{k}}{2\Delta\xi},$$
$$\frac{\partial T}{\partial z}=\frac{T_{i+1,j}^{k}-T_{i-1,j}^{k}}{2\Delta z},\ \frac{\partial^2 T}{\partial z^2}=\frac{T_{i+1,j}^{k}-2T_{i,j}^{k}+T_{i-1,j}^{k}}{(\Delta z)^2},$$
$$\frac{\partial c}{\partial t}=\frac{c_{i,j}^{k+1}-c_{i,j}^{k}}{\Delta t},\ \frac{\partial c}{\partial \xi}=\frac{c_{i,j+1}^{k}-c_{i,j-1}^{k}}{2\Delta\xi},$$
$$\frac{\partial c}{\partial z}=\frac{c_{i+1,j}^{k}-c_{i-1,j}^{k}}{2\Delta z},\ \frac{\partial^2 c}{\partial z^2}=\frac{c_{i+1,j}^{k}-2c_{i,j}^{k}+c_{i-1,j}^{k}}{(\Delta z)^2},\ \text{etc.}$$

The equations (31), (20) and (21) are now discretized following these finite difference approximations to the following difference equations given by

$$w_{i,j}^{k+1}=w_{i,j}^{k}+\Delta t\left[A_{i,j}^{k}\left(\frac{w_{i,j+1}^{k}-w_{i,j-1}^{k}}{2\Delta\xi}\right)+B_{i,j}^{k}\left\{\frac{w_{i,j+1}^{k}-2w_{i,j}^{k}+w_{i,j-1}^{k}}{(\Delta\xi)^2}\right\}\right.$$
$$\left.+\frac{\mu}{\rho}\left\{\frac{w_{i+1,j}^{k}-2w_{i,j}^{k}+w_{i-1,j}^{k}}{(\Delta z)^2}\right\}-w_{i,j}^{k}\left(\frac{w_{i+1,j}^{k}-w_{i-1,j}^{k}}{2\Delta z}\right)\right], \tag{32}$$

$$T_{i,j}^{k+1}=T_{i,j}^{k}+\Delta t\left[C_{i,j}^{k}\left(\frac{T_{i,j+1}^{k}-T_{i,j-1}^{k}}{2\Delta\xi}\right)-\frac{w_{i,j}^{k}}{2\Delta z}(T_{i+1,j}^{k}-T_{i-1,j}^{k})\right.$$
$$+D_{i,j}^{k}\left\{\frac{T_{i,j+1}^{k}-2T_{i,j}^{k}+T_{i,j-1}^{k}}{(\Delta\xi)^2}\right\}+\frac{k}{\rho c_p}\left\{\frac{T_{i+1,j}^{k}-2T_{i,j}^{k}+T_{i-1,j}^{k}}{(\Delta z)^2}\right\}$$
$$+\frac{2\mu}{\rho c_p}\left\{E_{i,j}^{k}\left(\frac{w_{i,j+1}^{k}-w_{i,j-1}^{k}}{2\Delta\xi}\right)+F_{i,j}^{k}\left(\frac{w_{i,j+1}^{k}-2w_{i,j}^{k}+w_{i,j-1}^{k}}{(\Delta\xi)^2}\right)\right.$$
$$+\frac{w_{i+1,j}^{k}-2w_{i,j}^{k}+w_{i-1,j}^{k}}{(\Delta z)^2}-J_{i,j}^{k}\left(\frac{u_{i,j+1}^{k}-u_{i,j-1}^{k}}{2\Delta\xi}\right)$$
$$\left.\left.+\frac{1}{R_i^{k}}\left(\frac{u_{i,j+1}^{k}-2u_{i,j}^{k}+u_{i,j-1}^{k}}{(\Delta\xi)^2}\right)+\frac{u_{i+1,j}^{k}-u_{i-1,j}^{k}}{2\Delta z}\right\}\right] \tag{33}$$

and

$$c_{i,j}^{k+1}=c_{i,j}^{k}+\Delta t\left[H_{i,j}^{k}\left(\frac{c_{i,j+1}^{k}-c_{i,j-1}^{k}}{2\Delta\xi}\right)+I_{i,j}^{k}\left(\frac{c_{i,j+1}^{k}-2c_{i,j}^{k}+c_{i,j-1}^{k}}{(\Delta\xi)^2}\right)\right.$$
$$-w_{i,j}^{k}\left(\frac{c_{i+1,j}^{k}-c_{i-1,j}^{k}}{2\Delta z}\right)+D\left(\frac{c_{i+1,j}^{k}-2c_{i,j}^{k}+c_{i-1,j}^{k}}{(\Delta z)^2}\right)$$
$$+\frac{Dk_T}{T_m}\left\{M_{i,j}^{k}\left(\frac{T_{i,j+1}^{k}-T_{i,j-1}^{k}}{2\Delta\xi}\right)+N_{i,j}^{k}\left(\frac{T_{i,j+1}^{k}-2T_{i,j}^{k}+T_{i,j-1}^{k}}{(\Delta\xi)^2}\right)\right.$$
$$\left.\left.+\left(\frac{T_{i+1,j}^{k}-2T_{i,j}^{k}+T_{i-1,j}^{k}}{(\Delta z)^2}\right)\right\}\right], \tag{34}$$

where the respective coefficients $A_{i,j}^{k}$, $B_{i,j}^{k}$, $C_{i,j}^{k}$ involving (32)-(34) have got their expressions included in Appendix. The discretisation needs to be performed by defining $z_i=(i-1)\Delta z$, $i=1(1)M+1$ and $\xi_j=(j-1)\Delta\xi$, $j=1(1)N+1$ for the entire bifurcated arterial segment under consideration where Δz and $\Delta\xi$ are the respective increments in the axial and the radial directions. The initial and the boundary conditions (22)-(28) are also discretized in a similar manner as follows :

$$u_{i,j}^{1}=u_0,\ w_{i,j}^{1}=w_0,\ T_{i,j}^{1}=T_0 \ \text{ for all } i,j \tag{35}$$

$$u_{i,1}^{k}=0,\ w_{i,2}^{k}=w_{i,1}^{k} \ \text{ for } z_i\le z_3 \tag{36}$$

$$u_{i,N+1}^{k}=\alpha\frac{\partial R_{1i}^{k}}{\partial t},\ w_{i,N+1}^{k}=0 \ \text{ for all } z_i \tag{37}$$

$$u_{i,1}^{k}=\alpha\frac{\partial R_{2i}^{k}}{\partial t},\ w_{i,1}^{k}=0 \ \text{ for } z_i\ge z_3 \tag{38}$$

$$T_{i,2}^{k}=T_{i,1}^{k},\ c_{i,2}^{k}=c_{i,1}^{k} \ \text{ for } z_i\le z_3 \tag{39}$$

$$c_{1,j}^{k}=c_0,\ c_{M+1,j}^{k}=c_{M,j}^{k} \ \text{ for all } j \tag{40}$$

$$\text{and } T_{i,1}^{k}=T_1 \ \text{ for all } i,k. \tag{41}$$

After having obtained the solution of (32) using the relevant conditions numerically for the axial velocity component of the blood flow, the corresponding radial velocity can be directly determined from (30). Subsequently, the temperature distribution describing heat transfer can be obtained from (33) which requires the results of the flow-field already evaluated numerically. The mass concentration describing the mass transfer can finally be quantified by making use of the results obtained in the first two phases mentioned above. The volumetric flow rate or the net flux of blood for both the parent aorta ($z\le z_3$) and the daughter ($z\ge z_3$) arteries can be determined by following the truncated Taylor's series expansions to express the velocity field in the daughter arteries along the oblique line inclined at an angle β with the trunk axis, given by

$$u_{i,j}^{k}{}'=u_{i,j}^{k}-\frac{\partial u_{i,j}^{k}}{\partial z}(j-1)\Delta\xi\tan\beta+\frac{1}{2}\frac{\partial^2 u_{i,j}^{k}}{\partial z^2}[\Delta\xi(j-1)\tan\beta]^2+\cdots\cdots \tag{42}$$

$$w_{i,j}^{k}{}'=w_{i,j}^{k}-\frac{\partial w_{i,j}^{k}}{\partial z}(j-1)\Delta\xi\tan\beta+\frac{1}{2}\frac{\partial^2 w_{i,j}^{k}}{\partial z^2}[\Delta\xi(j-1)\tan\beta]^2+\cdots\cdots \tag{43}$$

and consequently their discretised versions with first order approximation give

$$u_{i,j}^{k}{}'=u_{i,j}^{k}-\left(\frac{j-1}{2\Delta z}\right)(u_{i+1,j}^{k}-u_{i-1,j}^{k})\Delta\xi\tan\beta+O(h^2), \tag{44}$$

$$w_{i,j}^{k}{}'=w_{i,j}^{k}-\left(\frac{j-1}{2\Delta z}\right)(w_{i+1,j}^{k}-w_{i-1,j}^{k})\Delta\xi\tan\beta+O(h^2), \tag{45}$$

h being the width of the mesh.

Hence the volumetric flow rate (Q) of the fluid can be defined as $Q=Q_p+Q_d$ in which Q_p represent the flow rate for the parent ($z\le z_3$) aorta and Q_d, the net flux for the daughter ($z\ge z_3$) arteries whose respective expressions should be read as

$$Q_p = 2\pi R_i^k \left[R_i^k \int_0^1 \xi_j w_{i,j}^k d\xi + R_{2i}^k \int_0^1 w_{i,j}^k d\xi \right], \tag{46}$$

$$\begin{aligned} Q_d = & -\pi (R_i^k)^2 \int_0^{\frac{\sec\beta}{2}} \xi_j (w_{i,j}^k{}' \cos\beta + u_{i,j}^k{}' \sin\beta) d\xi_j \\ & - \pi R_i^k R_{2i}^k \int_0^{\frac{\sec\beta}{2}} (w_{i,j}^k{}' \cos\beta + u_{i,j}^k{}' \sin\beta) d\xi_j \\ & + \pi (R_i^k)^2 \int_{\frac{\sec\beta}{2}}^{\sec\beta} \xi_j (w_{i,j}^k{}' \cos\beta + u_{i,j}^k{}' \sin\beta) d\xi_j \\ & + \pi R_i^k R_{2i}^k \int_{\frac{\sec\beta}{2}}^{\sec\beta} (w_{i,j}^k{}' \cos\beta + u_{i,j}^k{}' \sin\beta) d\xi_j \end{aligned} \tag{47}$$

From the temperature field equation (33) one can obtain the heat flux (Q_T) or the rate of heat transfer as

$$Q_T = \frac{-k\partial T}{R\,\partial\xi}\bigg|_{\xi=1} = \frac{-k}{\Delta\xi R_i^k}(T_{i,N+1}^k - T_{i,N}^k), \tag{48}$$

while the diffusion rate (Q_c) or the rate of mass transfer can be determined from the concentration field equation (34) as

$$Q_c = \frac{-D\partial c}{R\,\partial\xi}\bigg|_{\xi=1} = \frac{-D}{2\Delta\xi R_i^k}(c_{i,N+1}^k - c_{i,N-1}^k), \tag{49}$$

6. Numerical results and discussion

For the purpose of the applicability of the present mathematical model, a specific numerical illustration has been taken by making use of the available data for all the physical parameters involved in the present analysis. The large scale numerical computations have been performed with a view to estimate quantitatively the unsteady profiles of the velocity field, temperature field and the mass concentration together with the distributions of the flow rate, the heat flux and the diffusive flux over the entire bifurcated arterial segment under consideration. The influences of the arterial constrictions and the wall motion on these results are also recorded quantitatively. The following tabular data have been made use of for the purpose of the numerical computations (cf. Milnor, 1982; Lou and Yang, 1992; Rappitsch and Perktold, 1996; Friedman and Ehrlich, 1975) :

Table 1. Data for various physical parameters

$a = 11$ mm	$l_0 = 15$ mm, $d = 5$ mm	$z_{max} = 60$ mm
$\tau_m = 0.3a$	$f_p = 1.2$ Hz	$\beta = 45^\circ$
$\rho = 1.05 \times 10^3$ Kg m^{-3}	$\mu = 0.0035$ Nm^{-2}s	$r_1 = 0.7a$
$k_1 = 0.1$	$z_1 = 10$ mm	$z_5 = 40$ mm
$D = 1.6 \times 10^{-4}$ mm^2 s^{-1}	$A_0 = 10$ kg m^{-2} s^{-2}	$A_1 = 0.2A_0$
$c_0 = 2.58 \times 10^{-6}$ m*l* mm^{-3}	$k = 0.5$ W m^{-1} K^{-1}	$k_T = 0.15 \times 10^{-6}$
$T_m = 310^\circ$K	$T_1 = 309^\circ$K	$c_p = 3900$ J Kg^{-1} K^{-1}

The finite difference scheme adopted here for solving (32) as the first step towards numerical computation does converge with the desired degree of accuracy for the respective spacings $\Delta z = 1.0$ and $\Delta\xi = 0.01$ along the axial and the radial directions. These results are subsequently made use of to solve the remaining equations (30), (33) and (34) numerically. The converged results for a grid size of 60×100 for various quantities of interest are displayed through the Figs. 2-26 followed by scientific discussions so as to validate the applicability of the present model. For the purpose of understanding the behaviour of the various results of interest, the following subsections properly titled in view of keeping an insight into the relevant discussion over the results obtained.

6.1. Flow profiles of the velocity field in the parent aorta and daughter artery

Fig. 2 illustrates the patterns of the axial velocity profile

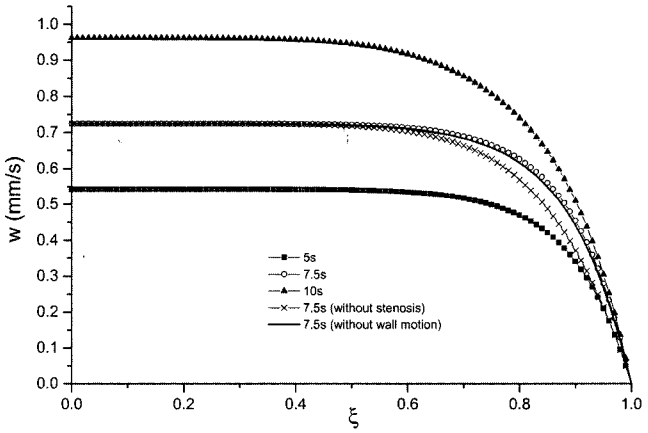

Fig. 2. Axial velocity profile for the parent aorta at the maximum constricted site ($z = 6$ mm) for different time periods.

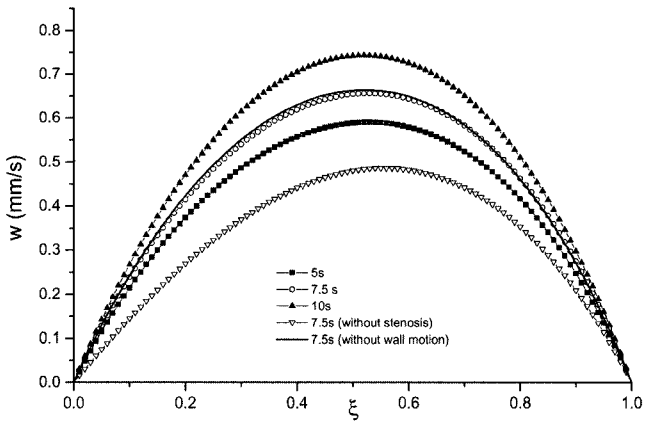

Fig. 3. Axial velocity profile for the daughter artery at the throat of the stenosis ($z = 45$ mm) for different time periods.

of the streaming blood in the parent aorta at a specific location of $z = 6$ mm where it assumes its constriction maximum for three different time periods while those in the daughter artery at its constriction site of $z = 45$ mm are presented in Fig. 3. Both the figures also include the corresponding results obtained by disregarding the presence of constriction in one case and by neglecting the arterial wall motion in another treatment. The parabolic velocity profiles in the parent aorta appear to diminish from their maxima at the axis as one moves away from it and finally they approach a minimum value on the wall surface where the flow velocity completely merges with the velocity of the moving arterial wall. On the other hand, the flow patterns in the daughter artery change drastically from parabolic to symmetrical type about the mid-surface between the inner and the outer wall of the branch artery. The unsteady nature of the axial velocity of the streaming blood appears to have resemblance in both the parent and its daughter arteries in a sense that the velocity gets enhanced with the advancement of time. The effect of arterial wall motion on the velocity happens to be meagre while that of the stenoses on the velocity in both the parent and the daughter arteries is significant. The absence of the constriction causes a reduction of the velocity over the entire radial region of the daughter artery while such reduction appears only over a small area in the vicinity of the outer wall of the parent aorta.

Unlike the nature of the axial velocity profile of the flowing blood, the results of the radial velocity component at those critical locations of the parent and the daughter arteries presented in Figs. 4 & 5 are noted to be all time negative. In the parent aorta, the radial velocity declines from zero on the axis as one moves away from it and eventually to increase towards the wall to attain some finite value on the wall surface. The results do shift towards the origin as time progresses. Conversely, in the daughter artery, all the

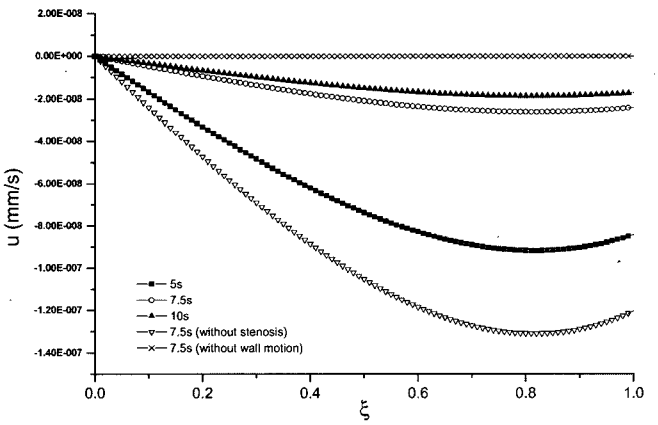

Fig. 4. Radial velocity profile for the parent aorta at the maximum constricted site ($z = 6$ mm) for different time periods.

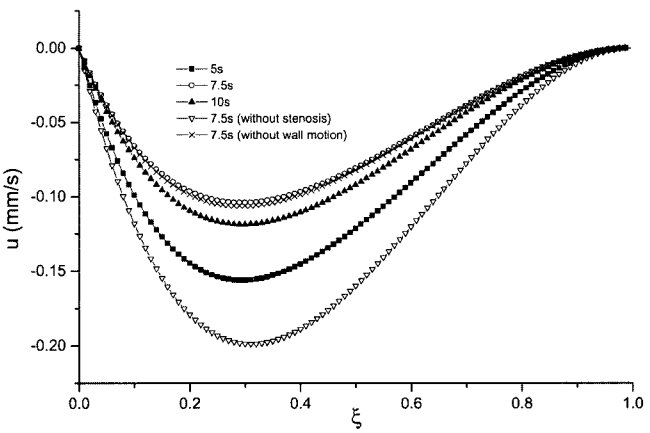

Fig. 5. Radial velocity profile for the daughter artery at the throat of the stenosis ($z = 45$ mm) for different time periods.

curves representing radial velocities drop from zero on the inner wall surface, attain their maxima at a short distance away from the inner wall and then rise to become zero again on the outer wall surface. The pulsatile nature of the profiles reflects the unsteady behaviour of the radial velocity in the daughter artery. When the wall motion is totally withdrawn, that is, for a rigid artery, the velocity profile gets perturbed more in the parent aorta and less in the daughter one. In the absence of any arterial constriction, the deviations of the result in both the parent and its daughter artery are quite significant and hence the effects of stenoses on the radial velocity profile of the stream can be estimated quantitatively. It may be of some importance to record that the magnitudes of the radial velocity are greatly enhanced in the branch artery than those in the main aorta but these are, however, quite smaller in magnitude than those of the axial velocity.

6.2. Temperature profiles in the parent aorta and its branches

Figs. 6 and 7 represent the respective temperature profiles in the parent aorta at its maximum constricted site ($z = 6$ mm) and at the apex ($z = z_3$) for different time periods. The parabolic profile of the temperature remains unperturbed with time advancement in the main aorta and it is also not influenced by the presence of constriction and the wall motion. However, the temperature profile changes its pattern at the apex which eventually gets perturbed to some extent for enhancement of time from $t = 5$ s to 7.5 s and from 7.5 s to 10 s as noted in Fig. 7. All the curves representing the temperature profile at the apex increase a little from the mean temperature of blood and thereafter diminish to attain finally the temperature of the inner wall. Here , the apex of the arterial bifurcation experiences meagre influences of the arterial constriction and the arterial wall motion as well on the temperature profile.

The temperature profiles of the daughter artery in the

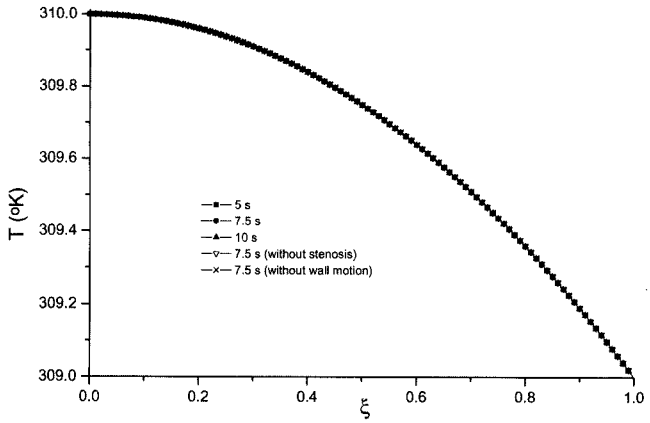

Fig. 6. Temterature profile for the parent aorta at the maximum constricted site ($z = 6$ mm) not influenced by the stenosis, wall motion and time.

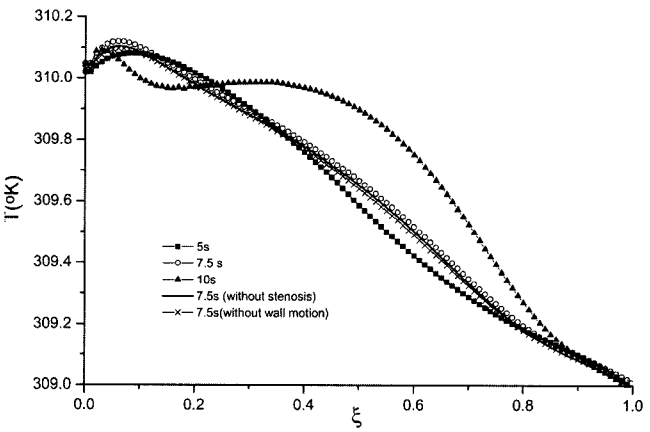

Fig. 7. Temperature profile for the apex ($z = z_3$) for different time periods.

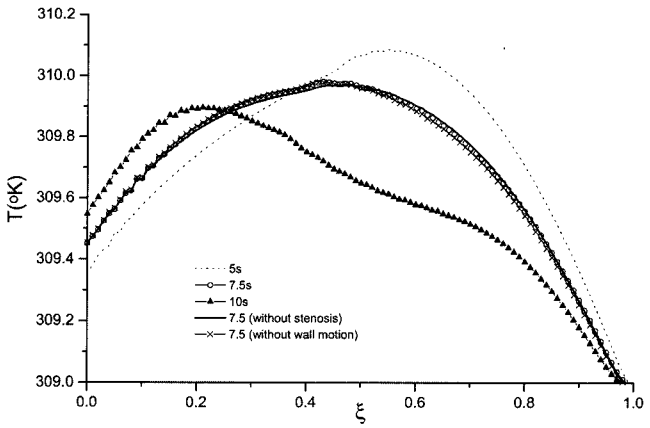

Fig. 8. Temperature profile for the daughter artery at the prestenotic region ($z = 40$ mm) for different time periods.

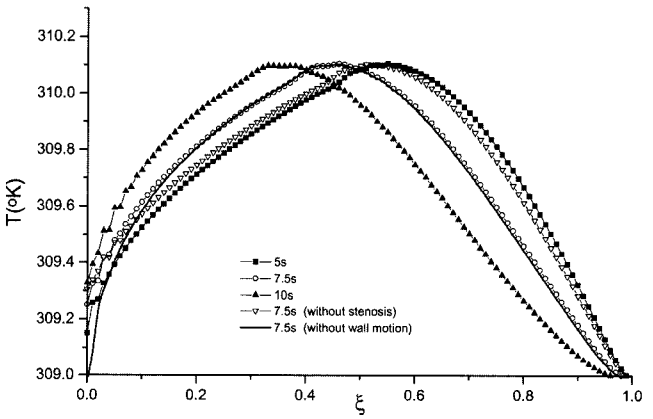

Fig. 9. Temperature profile for the daughter artery at the throat of the stenosis ($z = 45$ mm) for different time periods.

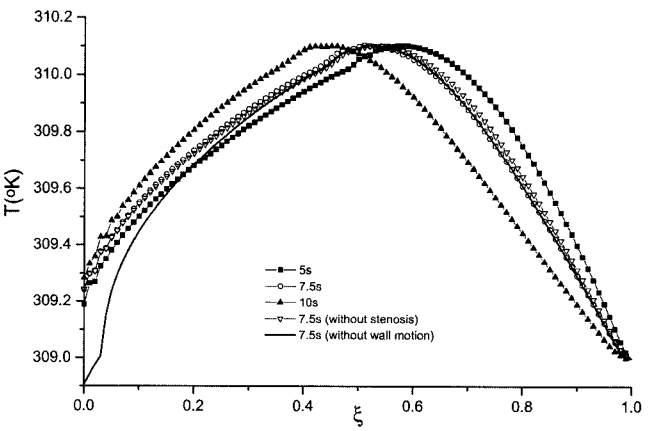

Fig. 10. Temperature profile for the daughter artery at the post stenitic region ($z = 51$ mm) for different time periods.

unsteady state at three different locations of $z = 40$ mm, 45 mm and 51 mm corresponding to pre-stenotic , stenotic and post-stenotic regions are exhibited in Figs. 8-10. These figures also include the results corresponding to three different time periods and the results computed by disregarding the presence of constriction and the wall motion from the present dynamical system. The unsteady behaviour of the temperature profiles indicates that at the prestenotic region, the maximum temperature occurs at $t = 5$ s just right of the mid surface which diminishes at $t = 7.5$ s and 10 s and the peaks do shift towards the inner wall vicinity while the magnitudes of the peaks corresponding to different time periods remain same but they appear in the neighborhood of the mid surface in the case of stenotic and post-stenotic regions. One may record that the effect of constriction on the temperature profile in the daughter artery at the throat of the stenosis appears to be quite significant unlike that in the pre-stenotic and the post-stenotic regions. The influence of wall motion on temperature is however found to be negligible in the daughter artery.

Fig. 11 displays the results of the distribution of temperature in the daughter arterial segment for various radial

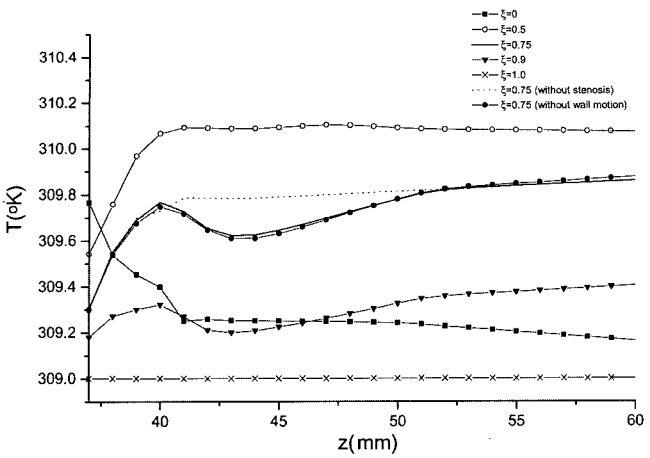

Fig. 11. Temperature distribution in the daughter artery for different radial positions at $t = 5$ s.

positions at a particular instant of $t = 5$ s including those corresponding to the absence of constriction and the absence of wall motion. The inner wall of the daughter artery experiences a reduction of the distribution of the temperature over the entire arterial segment while the outer wall attains a constant uniform temperature represented by the bottom most curve. The mid surface, however, gains maximum temperature distribution of all other radial locations of the daughter artery. The influence of constriction on the temperature distribution appears to be quite pronounced in a specified area covering the stenotic region of the daughter artery while that of the wall motion does not appear to affect the temperature distribution.

6.3. Concentration profiles of the solute in the parent aorta and its branches

The concentration profiles of the solute for the parent aorta at three specific locations viz. at the onset of the constriction, at the maximum constricted site and at the offset of the stenosis for different time periods are plotted in Figs. 12-14. All these curves appear to be diminishing from their respective maxima at the axis as one moves away from it and finally they approach a minimum value at a particular instant of time. The increasing trend of the concentration profile with the advancement of time reflects its behaviour in the unsteady state. The concentration level at the maximum constricted region increases significantly from those of upstream and downstream for all times excepting at $t = 10$ s where the upstream concentration becomes higher than that of the stenotic region. The concentration grows up faster in the stenotic region as the oxygen gets trapped more in the constricted region than in the unconstricted one. The results corresponding to non-constricted artery and the rigid artery at $t = 7.5$ s indicate that the presence of stenosis influences the concentration profile more significantly than that of the arterial wall distensibility.

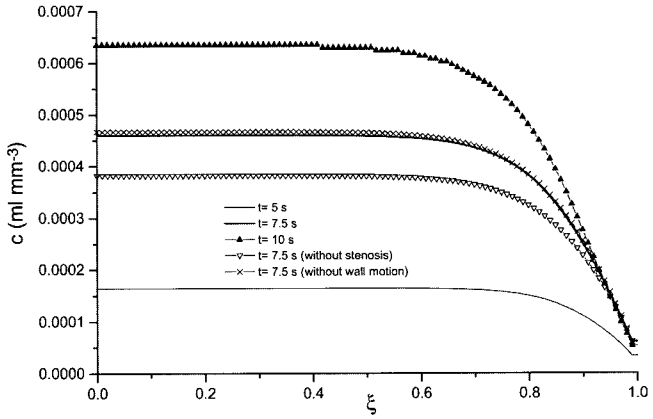

Fig. 12. The concentration profile for the parent aorta at the pre-stenotic region ($z = 4$ mm) for different time periods.

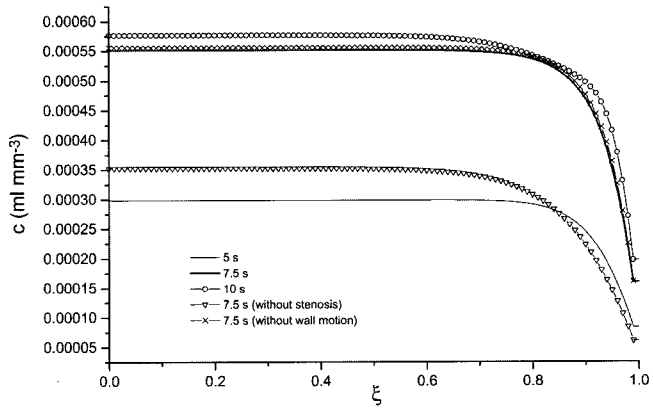

Fig. 13. The constriction profile for the parent aorta at the maximum constricted site ($z = 6$ mm) for different time periods.

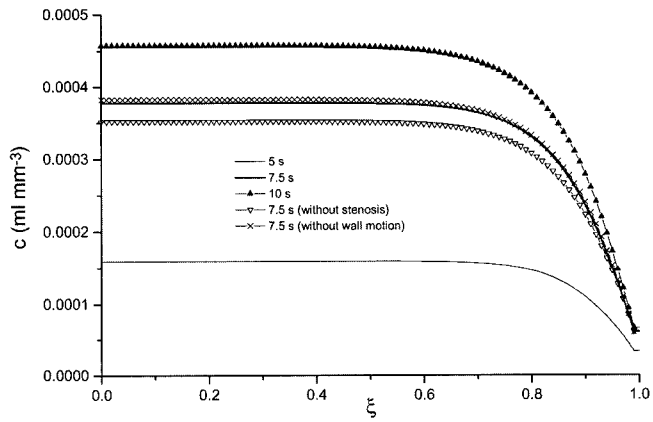

Fig. 14. The constriction profile for the parent aorta at the post-stenotic region ($z = 10$ mm) for different time periods.

Fig. 15 shows how the concentration profile of the solute gets distorted at the apex of the bifurcated artery for dif-

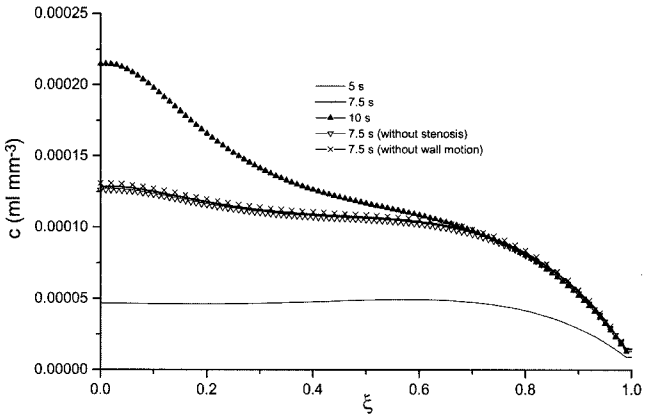

Fig. 15. The constriction profile at the apex ($z = z_3$) of the bifurcated artery for different time periods.

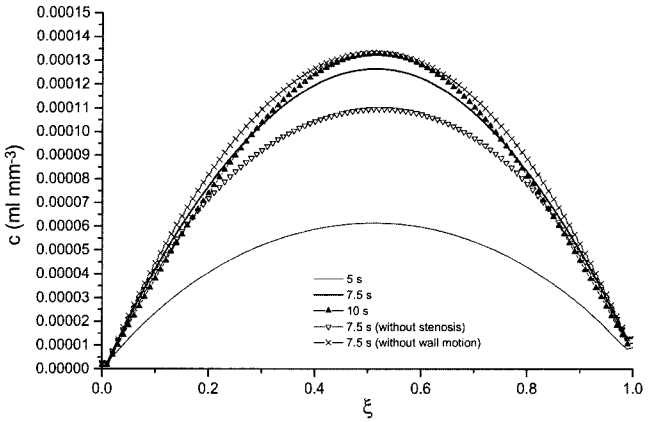

Fig. 16. The constriction profile for the daughter artery at the prestenotic region ($z = 40$ mm) for different time periods.

ferent time periods. The shape of the profile changes appreciably with the advancement of time from 5 s to 7.5 s and from 7.5 s to 10 s unlike those of Figs. 12-14. It may be noted here that the magnitudes of the concentration level are greatly lowered from those of the specific locations of the parent aorta. So, one may record that the concentration of the solute decays more at the apex than at any other locations of the parent duct. The effects of the stenosis and the vessel wall distensibility on the concentration profile are found to be insignificant at the apex.

The concentration profiles of the solute for the daughter artery in the unsteady state at three different locations of z = 40 mm, 45 mm and 51 mm corresponding to upstream the location of the stenosis, the stenotic region and to downstream the location of stenosis respectively, are portrayed in Figs. 16-18. The profiles presented in the daughter arteries appear to have different patterns from those of the mother one. The nearly symmetrical shape of the profile at the onset of the constriction gets perturbed more towards the outer wall as the flow advances to the constricted region and then to the downstream the location of the stenosis in the branch artery. The concentration levels in the daughter arteries fall significantly from those of the mother aorta, in general, and rise at the throat of the stenosis more than at the unconstricted sites of the daughter arteries, in particular. The unsteady behaviour of the profiles of the present figures is similar to those of Figs. 12- 14 in a sense that the concentration of the solute increases with time advancement. The considerable effect of constriction on the concentration profile can be observed in both the Figs. 16 and 17 while Fig. 18 indicates meagre influence of stenosis. One may note further that the influence of vessel wall distensibility appears to be quite appreciable on the concentration profile at all the chosen sites of the daughter artery unlike those of the parent ones.

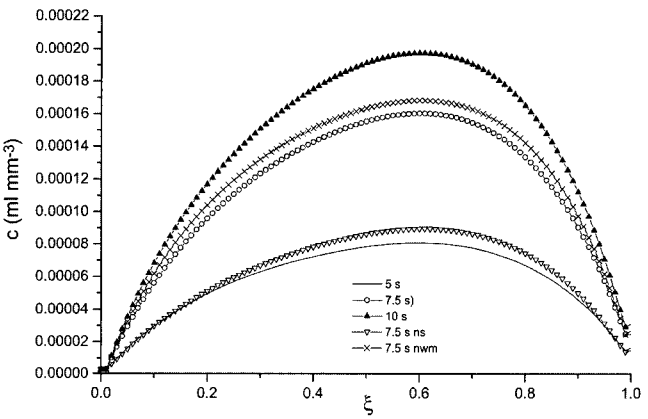

Fig. 17. The constriction profile for the daughter aretry at the throat of the stenosis ($z = 45$ mm) for different time periods.

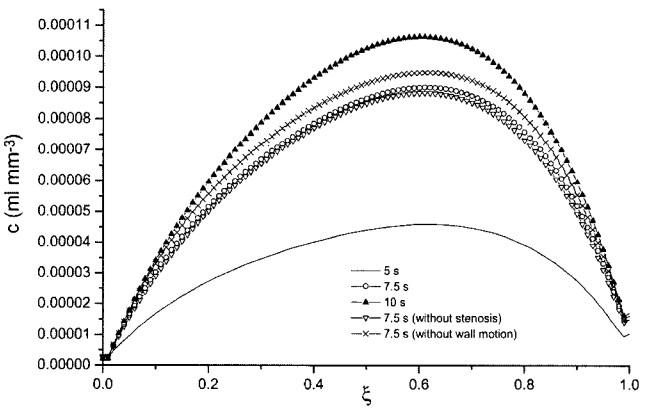

Fig. 18. The constriction profile for the daughter artery at the post-stenotic region for different time periods.

6.4. Blood flow rate and its distribution over the artery

Fig. 19 records the unsteady behaviour of the flow rate of

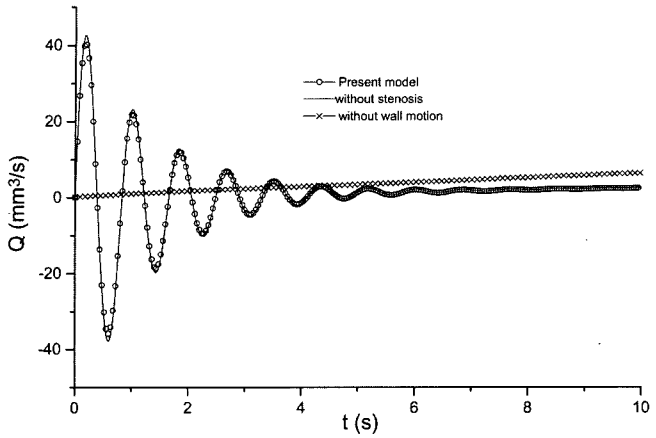

Fig. 19. Unsteady behaviour of the flow rate in the parent aorta at its maximum constriction site ($z = 6$ mm).

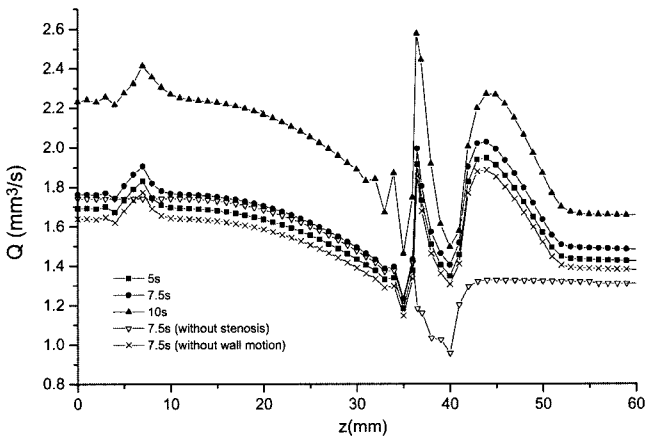

Fig. 20. Flux distribution of blood over the entire bifurcated arterial segment for different time periods.

the streaming blood in the parent aorta at its maximum constriction site for three different cases ---- first based on the present model, the second in the absence of stenosis and the third having no wall motion. The flow rate appears to get accelerated in the systolic phase and decelerated in the diastolic phase of the first cardiac cycle followed by similar fluctuations with gradually diminishing amplitudes for a few more cardiac cycles in succession and finally these fluctuations completely damp out for rest of the time. Such behaviour of the flow rate indicates back flow and several flow separation zones are formed as the direction of the flow rate changes from positive to negative, negative to positive and so on during the period of nearly six cardiac cycles. There is no significant influence of constriction recorded on the flow rate presented herein. If one disregards the wall motion, the nature of the flow rate changes drastically to show an all time increasing trend with much reduced magnitudes where no back flow takes place. Thus the vessel wall distensibility affects the flow rate significantly and its effect can be quantified through a direct comparison of the relevant curves of the present figure.

The flux distribution of the streaming blood over the entire bifurcated arterial segment in the unsteady state for three different time periods is recorded in Fig. 20. The present figure also includes the flow rate in the case of non-constricted artery and the rigid artery in order to examine their effects on the flux distribution of the streaming blood. Larger distribution occurs in the daughter artery than that of the parent aorta for all times and the peak flow rates are noted to appear at three specific locations --- one at the maximum constricted site of the mother artery, one at the onset of the daughter artery and another at the throat of the stenosis in the daughter artery. If one disregards the presence of constriction in both the parent aorta and its branch, the peaks disappear and the pattern of distribution alters largely in the daughter artery than in the parent aorta and the deviation thus obtained helps estimating the effect

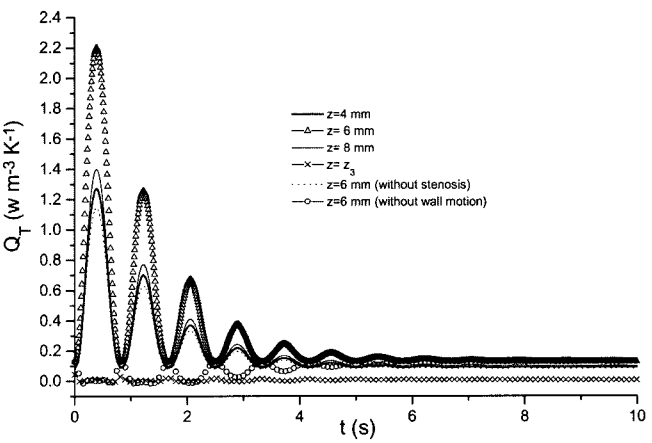

Fig. 21. Unsteady behaviour of the heat flux at the various locations of the parent aorta including the apex.

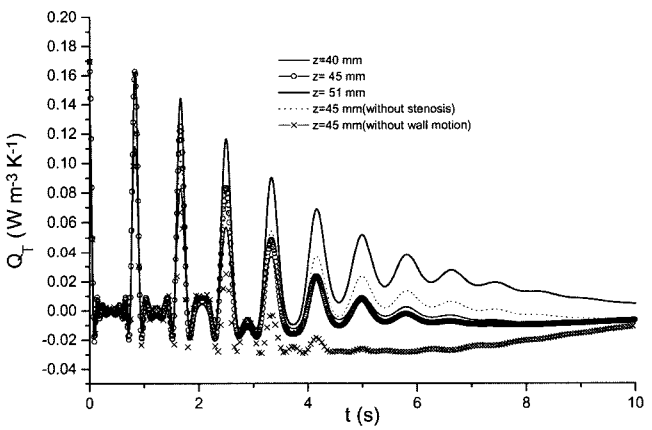

Fig. 22. Unsteady behaviour of the heat flux at different locations of the daughter artery.

of constriction on the flux distribution quantitatively. On the other hand, the arterial wall motion does not appear to have much influence on the flow rate distribution.

6.5. Rate of heat transfer and its distribution over the artery

Figs. 21 and 22 display the unsteady characteristics of the heat flux at various locations of the parent and daughter arteries including the apex. The undulating characteristics of the rate of heat transfer at all the chosen sites of the mother artery with gradually diminishing amplitudes completely damp out with the advancement of time especially after a few cardiac cycles. Such behaviour of the heat flux alters drastically at the apex ($z = z_3$) where the rate of heat transfer is reduced considerably to an uniform flux for all times. One may record from Fig. 21 that the constricted region experiences maximum heat flux compared to all other chosen sites of the parent aorta and the effect of stenosis on the rate of heat transfer becomes quite significant as evidenced from the deviation of the results corresponding to the constricted and non-constricted ones at $z = 6$ mm. When one disregards the wall motion of the artery, the nature of the heat flux reverses with lowered magnitudes for first several cardiac cycles until it merges completely with other curves for rest of the time. On the other hand, the scenario is different in the daughter artery where the curves representing the rate of heat transfer get largely distorted towards the beginning of a few cardiac cycles followed by undulating character with gradually diminishing amplitudes for the next few cycles and finally become steady towards the end of large passage of time. Here too, the influence of the stenosis and the wall motion on the heat flux are noted to be quite appreciable.

The distribution of the rate of the heat transfer over the entire bifurcated arterial segment for different time periods is exhibited in Fig. 23 inclusive of the corresponding results in the absence of arterial constrictions in one case and the absence of wall motion in other case. The behaviour of the heat flux distribution over the parent aorta appers to be analogous to those of the distribution of the flow rate presented in Fig. 20 but in the daughter artery, the rate of heat transfer is distributed differently in a way that it increases upstream the constriction. In the absence of arterial constrictions, the heat flux distribution remains constant in the daughter artery with reduced magnitude attained near the apex of the bifurcated artery. Hence one can estimate the effect of constrictions on the heat flux distribution quantitatively by comparing the relevant curves of the present figure. The present results also indicate however, that the arterial wall motion does not influence the rate of heat transfer over the arterial segment under consideration.

6.6. Wall diffusive flux of the solute and its distribution over the artery

The results of Fig. 24 illustrate the unsteady behaviour of the diffusive flux of the solute on the outer wall at various locations of the bifurcated arterial segment. In all the chosen sites of the artery excepting at the apex, the rate of mass transfer of the solute increases to begin with at the

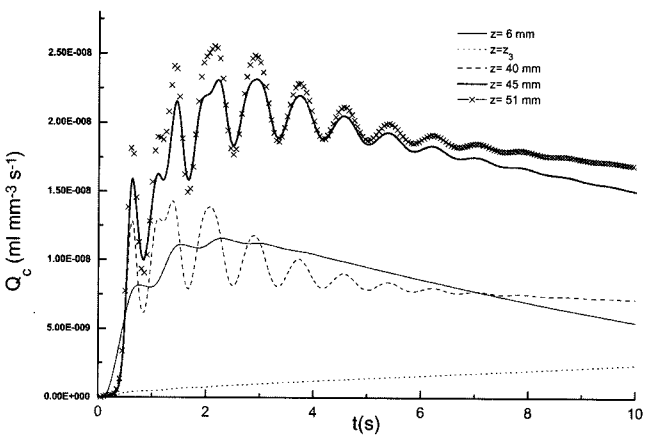

Fig. 24. Unsteady behaviour of the diffusive flux of the solute on the outer wall at different locations.

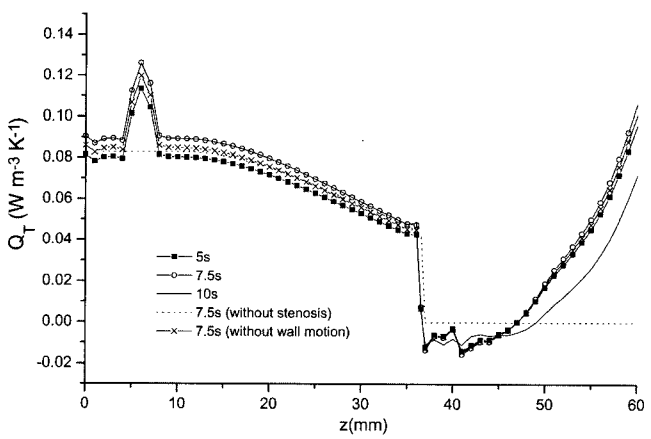

Fig. 23. Distribution of the rate of heat transfer over the entire bifurcated arterial segment for different time periods.

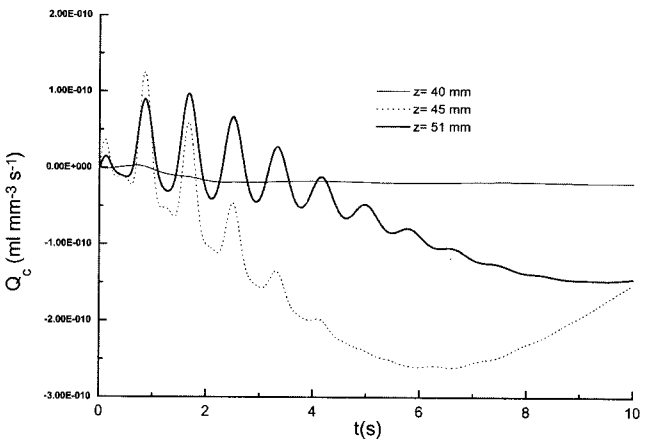

Fig. 25. Unsteady behaviour of the diffusive flux of the solute at different sites of the inner wall.

onset of the cardiac cycle followed by a few fluctuations with increasing trend and then gradually diminishes with a reduction of the amplitudes for rest of the time. The distortions in the behaviour of the rate of mass transfer on the outer wall appear more at all the specific sites of the daughter artery than in the parent aorta. The apex however, experiences no distortion in the diffusive flux which increases linearly with the advancement of time by keeping a low profile so far as the magnitudes are concerned. The transfer rate of the solute becomes higher towards the offset of the constriction than both at the onset and at the throat of the stenosis in the daughter arterial lumen. On the other hand, a reverse phenomena in the unsteady behaviour of the inner wall flux of the solute is depicted in Fig. 25 at those specific sites of the daughter artery. The diffusive flux on the inner wall at the onset ($z = 40$ mm) of stenosis appears to have several fluctuations forming ups and downs from positive to negative, negative to positive and so on with decreasing trend while at the offset ($z = 51$ mm) of constriction, it remains almost unperturbed with relatively lower magnitudes. The stenotic region ($z = 45$ mm) however experiences sequence of distortions with higher diminishing rate mostly in the negative sense. The negative flux indicates the back flow of the solute resulting from the constriction of the inner wall of the branch artery. The direction of the mass transfer alters from positive to negative as it approaches the arterial constriction which becomes almost all time negative at the throat of the constriction and finally assumes positive values the moment it crosses the constricted region. So, the effect of the stenosis on the diffusive flux of the solute appears to be quite substantial.

Finally, the concluding Fig. 26 of the present paper shows the distribution of the mass transfer of the solute at the outer wall of the entire bifurcated arterial segment at different time periods. The wall flux of the solute appears to have its maximum at the specific locations of maximum constrictions for all time where the mean concentration of solute is high. One may note that the high diffusive flux at the wall means that the concentration gradient is high which results in a low concentration of the solute at the wall compared with the streaming blood if the direction of the flux is outwards as in the present case. The present results agree qualitatively well with Back *et al.* (1997) who found a peak in wall flux just upstream the location of maximum constriction.

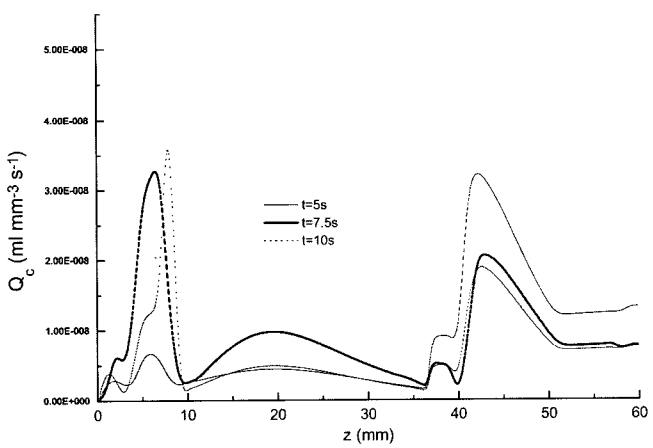

Fig. 26. Diffusive flux distribution of the solute at the outer wall over the entire arterial segment for different time periods.

7. Concluding remarks

A mathematical model for unsteady heat and mass transfer in blood flow through a stenosed bifurcated artery has been developed. Special emphasis has been put on the motion of the arterial wall and its effect on local fluid mechanics but not on the stresses and strains of the wall. The flow mechanism has been made governed by an input pulsatile pressure gradient. The influences of stenose present both in the mother and daughter arterial lumen and the wall distensibility on the velocity, temperature and the concentration profiles, the fluid flux, the heat flux and the diffusive flux of the solute are all examined quantitatively in order to validate the applicability of the model under consideration. The salient observations of the present theoretical study are listed below :

- The pattern of the velocity profile of the streaming blood alters in the daughter artery from that in the parent one and the magnitudes of the radial velocity are smaller than those of axial velocity.
- The arterial wall distensibility causes the radial velocity of the streaming blood in the duct to alter its direction but that in the daughter artery remains unperturbed.
- There are appreciable influences of stenoses on the velocity field of the flowing blood, the concentration profile of the solute in the entire bifurcated artery in general and on the temperature profile at the throat of the constricted daughter artery, in particular.
- The undulating characteristics of the flow rate with time engineer back flow and help in the formation of several flow separation zones for some cardiac cycles which subsequently damp out beyond $t = 6$ s.
- The oscillatory behaviour of the heat flux with gradually diminishing amplitudes in the mother artery damps out to become steady after $t = 6$ s and the amplitudes are substantially shrinked down in the absence of arterial constriction. There is also a considerable reduction of magnitude of the heat flux when the arterial wall distensibility is disregarded.
- The diffusive flux of the solute on the outer wall appears to enhance more in the branch artery than in parent aorta for all times while that on the inner wall

alters from positive to negative, that means, the direction of the mass transfer changes in the inner wall of the daughter artery unlike that on the outer wall.
- The presence of the arterial constrictions causes significant effects on the flux distribution of the streaming blood and the rate of the heat transfer more towards the daughter artery than its mother one.
- The peak rates of mass transfer appear at both the constricted sites of the parent and its daughter artery.

Acknowledgements

Authors are highly grateful to the reviewers for their valuable comments and suggestions. The present work is part of the special Assistance Programme [Grant No. F.510/8/DRS/ 2004(SAP-I)] sponsored by the University Grants Commission (UGC), New Delhi, India.

References

Ahmed, M. E. S. and H. A. Attia, 1998, Magnetohydrodynamic flow and heat transfer of a non-Newtonian fluid in an eccentric annulus, *Cand. J. Phys.* **76**, 391-401

Back, L. H., J. R. Radbill and D. W. Crawford, 1997, Analysis of oxygen transport from pulsatile, viscous blood flow in diseased coronary arteries of man, *J. Biomech.* **10**, 763-774.

Barozzi, G. S. and A. Dumas, 1991, Convective heat transfer coefficients in the circulation, *J. Biomech. Engng.* **113**, 308-313.

Friedman, M. H. and L. W. Ehrlich, 1975, Effects of spatial variations in shear on diffusion at the wall of an arterial branch, *Cric. Res.* **37**, 446-454.

Chakravarty, S. and P. K. Mandal, 1997, An analysis of pulsatile flow in a model aortic bifurcation, *Int. J. Engng. Sci.* **35**, 409-422.

Charm, S, B. Paltiel and G. S. Kurland, 1968, Heat transfer coefficients in blood flow, *Biorheology* **5**, 133-145.

Chato, J. C., 1980, Heat Transfer to blood vessels, *Transc. ASME* **102**, 110-118.

Deshpande, M., D. Giddens and R. Mabon, 1976, Steady flow through modelled vascular stenoses, *J. Biomech.* **9**, 165-174.

Friedman, M. H. and L. W. Ehrlich, 1975, Effects of spatial variations in shear on diffusion at the wall of an arterial branch, *Cric. Res.* **37**, 446-454.

Hung, I. C. and Y. Perng, 1991, Flow of non-Newtonian fluid in the entrance region of a tube with porous walls, *Int. J. Heat Fluid Flow* **12**, 263-268.

Imaeda, K. and F. O. Goodman, 1980, Analysis of nonlinear pulsatile blood flow in arteries, *J. Biomech.* **13**, 1007-1022.

Kawase, Y. and J. J. Ulbrecht, 1983, Heat and Mass Transfer in Non-Newtonian Fluid Flow with Power Function Velocity Profiles, *Can. J. Chem. Eng.* **61**, 791-800.

Lagendijk, J. J. W., 1982, The influence of blood flow in large vessels on the temperature distribution in hyperthemia, *Phys. Med. Biol.* **27**, 17-23.

Ling, S. C. and H. B. Atabek, 1972, A nonlinear analysis of pulstile blood flow in arteries, *J. Fluid Mech.* **55**, 492-511.

Lou. Z. and W. J. Yang, 1992, Biofluid dynamics at arterial bifurcations, *Crit. Rev. Biomed. Engng.* **19**, 455-493.

Ma, P., X. Li and D. N. Ku, 1994, Heat and mass transfer in a separated flow region for high Prandtl and Schmidt numbers under pulsatile conditions, *Int. J. Heat and Mass Transfer* **37**, 2723-2736.

Mathur, M. N. and R. K. Bhatnagar, 1967, *ZAMM* **47**, 379.

Milnor, W. R., 1982, Hemodynamics, Williams and Williams, Baltimore.

Parikh, R. S. and R. Mahalingam, 1988, Int. comm.. Heat Mass Transfer **15**, 1.

Pedley, T. J., 1980, The fluid Mechanics of Large Blood Vessels, Cambridge University Press, Cambridge.

Pereira, E. C., M. Bhattacharya and R. V. Morey, 1989, *Transc. ASME* **32**, 256.

Rappitsch, G. and K. Perktold, 1996, Computer simulation of convective diffusion processes in large arteries, *J. Biomech.* **39**, 207-215.

Victor, S. A. and V. L. Shah, 1975, Heat transfer to blood flowing in a tube, *Biorheology* **12**, 361-368.

Victor, S. A. and V. L. Shah, 1976, Steady state heat transfer to blood flowing in the entrance region of a tube, *Int. J. Heat and Mass Transfer* **19**, 777-783.

Womersley, J. R., 1957, An elastic tube theory of pulse transmission and oscillatory flow in mammalian arteries, Wright Air Development Centre Technical Report TR 56-6114.

Appendix

The discretised expressions of the coefficients $A^k_{i,j}$, $B^k_{i,j}$, $C^k_{i,j}$ etc. involved in (32), (33) and (34) should be read as

$$A^k_{i,j}=-\frac{1}{\rho}\left(\frac{\partial p}{\partial z}\right)^k_i+\frac{1}{R^k_i}\left[\xi_j\left(\frac{\partial R}{\partial t}\right)^k_i+\left(\frac{\partial R_2}{\partial t}\right)^k_i+\frac{\mu}{\rho(\xi_j R^k_i+R^k_{2i})}\right.$$
$$-\frac{\mu}{\rho}\left\{\left(\frac{\partial^2 R_2}{\partial z^2}\right)^k_i+\xi_j\left(\frac{\partial^2 R}{\partial z^2}\right)^k_i-\frac{2}{R^k_i}\left(\frac{\partial R}{\partial z}\right)^k_i\left[\xi_j\left(\frac{\partial R}{\partial z}\right)^k_i+\left(\frac{\partial R_2}{\partial z}\right)^k_i\right]\right\}$$
$$\left.-\frac{R^k_{2i}}{\xi_j R^k_i+R^k_{2i}}\left[u^k_{i,1}+\xi^2_j\left\{\alpha\left(\frac{\partial R_1}{\partial t}\right)^k_i-\frac{R^k_{2i}}{R^k_{1i}}u^k_{i,1}\right\}(2-\xi^2_j)\right]\right],$$

$$B^k_{i,j}=\frac{\mu}{\rho(R^k_i)^2}\left[1+\left\{\xi_j\left(\frac{\partial R}{\partial z}\right)^k_i+\left(\frac{\partial R_2}{\partial z}\right)^k_i\right\}^2\right],$$

$$C^k_{i,j}=\frac{1}{R^k_i}\left[\xi_j\left(\frac{\partial R}{\partial t}\right)^k_i+\left(\frac{\partial R_2}{\partial t}\right)^k_i\right]\left[w^k_{i,j}+\frac{2k}{\rho c_p R^k_i}\left(\frac{\partial R}{\partial z}\right)^k_i\right]$$
$$+\frac{1}{R^k_i}\left[\xi_j\left(\frac{\partial R}{\partial t}\right)^k_i+\left(\frac{\partial R_2}{\partial t}\right)^k_i\right]-\frac{u^k_{i,j}}{R^k_i}$$
$$+\frac{2k}{\rho c_p R^k_i}\left[\frac{1}{\xi_j R^k_i+R^k_{2i}}-\left\{\xi_j\left(\frac{\partial^2 R}{\partial z^2}\right)^k_i+\left(\frac{\partial^2 R_2}{\partial z^2}\right)^k_i\right\}\right],$$

$$D^k_{i,j}=\frac{k}{\rho c_p(R^k_i)^2}\left[1+\left\{\xi_j\left(\frac{\partial R}{\partial z}\right)^k_i+\left(\frac{\partial R_2}{\partial z}\right)^k_i\right\}^2\right],$$

$$E_{i,j}^k = \frac{2}{(R_i^k)^2}\left[\xi_j\left(\frac{\partial R}{\partial z}\right)_i^k + \left(\frac{\partial R_2}{\partial z}\right)_i^k\right]\left(\frac{\partial R}{\partial z}\right)_i^k - \frac{1}{R_i^k}\left[\xi_j\left(\frac{\partial^2 R}{\partial z^2}\right)_i^k + \left(\frac{\partial^2 R_2}{\partial z^2}\right)_i^k\right] + \frac{1}{R_i^k},$$

$$F_{i,j}^k = \frac{1}{(R_i^k)^2}\left[\xi_j\left(\frac{\partial R}{\partial z}\right)_i^k + \left(\frac{\partial R_2}{\partial z}\right)_i^k\right], \quad J_{i,j}^k = \frac{1}{R_i^k}\left[\xi_j\left(\frac{\partial R}{\partial z}\right)_i^k + \left(\frac{\partial R_2}{\partial z}\right)_i^k\right],$$

$$H_{i,j}^k = \frac{1}{R_i^k}\left[\xi_j\left(\frac{\partial R}{\partial z}\right)_i^k + \left(\frac{\partial R_2}{\partial z}\right)_i^k\right]\left[1 + w_{i,j}^k - D + \frac{2D}{R_i^k}\left(\frac{\partial R}{\partial z}\right)_i^k\right] - \frac{u_{i,j}^k}{R_i^k} + \frac{D}{R_i^k\{\xi_j R_i^k + R_{2i}^k\}},$$

$$I_{i,j}^k = \frac{D}{(R_i^k)^2}\left[1 + \left\{\xi_j\left(\frac{\partial R}{\partial z}\right)_i^k + \left(\frac{\partial R_2}{\partial z}\right)_i^k\right\}^2\right],$$

$$M_{i,j}^k = \frac{2}{(R_i^k)^2}\left[\xi_j\left(\frac{\partial R}{\partial z}\right)_i^k + \left(\frac{\partial R_2}{\partial z}\right)_i^k\right]\left(\frac{\partial R}{\partial z}\right)_i^k - \frac{1}{R_i^k}\left[1 + \xi_j\left(\frac{\partial^2 R}{\partial z^2}\right)_i^k + \left(\frac{\partial^2 R_2}{\partial z^2}\right)_i^k - \frac{1}{\{\xi_j R_i^k + R_{2i}^k\}}\right],$$

$$N_{i,j}^k = \frac{1}{(R_i^k)^2}\left[1 + \left\{\xi_j\left(\frac{\partial R}{\partial z}\right)_i^k + \left(\frac{\partial R_2}{\partial z}\right)_i^k\right\}^2\right].$$